MEASUREMENTS OF THERMAL UPDRAFT INTENSITY OVER COMPLEX TERRAIN USING AMERICAN WHITE PELICANS AND A SIMPLE BOUNDARY-LAYER FORECAST MODEL

HARLAN D. SHANNON[1,⋆], GEORGE S. YOUNG[1], MICHAEL A. YATES[2], MARK R. FULLER[3] and WILLIAM S. SEEGAR[4]

[1]*Department of Meteorology, The Pennsylvania State University, University Park, Pennsylvania, U.S.A.;* [2]*Raptor Research Center, Boise State University, Boise, Idaho, U.S.A.;* [3]*Forest and Rangeland Ecosystem Science Center, U.S. Geological Survey, Boise, Idaho, U.S.A.;* [4]*Center for Conservation Research and Technology, University of Maryland, Baltimore County, Baltimore, Maryland, U.S.A.*

(Received in final form 12 November 2001)

Abstract. An examination of boundary-layer meteorological and avian aerodynamic theories suggests that soaring birds can be used to measure the magnitude of vertical air motions within the boundary layer. These theories are applied to obtain mixed-layer normalized thermal updraft intensity over both flat and complex terrain from the climb rates of soaring American white pelicans and from diagnostic boundary-layer model-produced estimates of the boundary-layer depth z_i and the convective velocity scale w_*. Comparison of the flatland data with the profiles of normalized updraft velocity obtained from previous studies reveals that the pelican-derived measurements of thermal updraft intensity are in close agreement with those obtained using traditional research aircraft and large eddy simulation (LES) in the height range of 0.2 to 0.8 z_i. Given the success of this method, the profiles of thermal vertical velocity over the flatland and the nearby mountains are compared. This comparison shows that these profiles are statistically indistinguishable over this height range, indicating that the profile for thermal updraft intensity varies little over this sample of complex terrain. These observations support the findings of a recent LES study that explored the turbulent structure of the boundary layer using a range of terrain specifications. For terrain similar in scale to that encountered in this study, results of the LES suggest that the terrain caused less than an 11% variation in the standard deviation of vertical velocity.

Keywords: Convective boundary layer, Cross-country soaring, Mixed-layer similarity, Soaring birds, Thermal intensity profile.

1. Introduction

Thermal updraft intensity may be defined as the average vertical velocity within a thermal updraft. Similarity theories for thermal updraft intensity over relatively homogenous terrain have been developed using large research aircraft and large eddy simulation (Greenhut and Khalsa, 1987; Young, 1988; Schumann and Moeng,

⋆ Corresponding address: U.S. Department of Agriculture, World Agricultural Outlook Board, Room 5133 South Building, 1400 Independence Ave., SW, Washington D.C. 20250-3812, U.S.A. E-mail: hshannon@oce.usda.gov

Boundary-Layer Meteorology **104:** 167–199, 2002.

1991). Although effective in collecting data along extended straight-line paths, the poor maneuverability and large turning radius of multi-engine research aircraft make it difficult to obtain numerous samples within a small geographic area. This problem is compounded by the tendency for these large aircraft to disturb the atmosphere in their wake, complicating efforts to obtain uncontaminated turbulence measurements through multiple passes. As a result, studies of the turbulence structure of the dry convective boundary layer over rapidly changing terrain have instead been undertaken using large eddy simulation (LES). The LES results of Gopalakrishnan et al. (2000) provide useful insight into the effect of complex terrain on the convective boundary layer. Observational data are, however, needed to verify LES performance in this regime. Given the flight path limitations of the large aircraft previously employed in obtaining such verification (e.g., Greenhut and Khalsa, 1982; Young, 1988), a new method is introduced here to measure thermal updraft intensity over complex terrain.

Unmanned aerial vehicles (UAVs) recently have been developed as a platform overcoming the limitations associated with the use of large aircraft in meteorological research (e.g., Holland et al., 1992; Langford and Emanuel, 1993; Bluth et al., 1996). UAVs are capable of achieving much higher flight path densities over small areas, compared with the much larger multi-engine aircraft employed in previous studies. Given the size and performance similarity between soaring birds and UAVs, soaring birds offer another potential means for gathering these data when the instrumentation aboard such aircraft are adapted to these birds. Furthermore, in contrast to UAVs that do not necessarily soar and glide, the avian platform is particularly appealing given the maneuverability of these birds and their propensity for soaring within thermal updrafts.

Previous studies have shown that birds can indeed be used to gather qualitative information on boundary-layer meteorological processes. For example, Huffaker (1897) first proved the existence of thermal updrafts based upon the observed behaviour of soaring birds. Woodcock (1940, 1975) later noted that gulls soar when atmospheric conditions support thermal development, but engage in powered (i.e., flapping) flight when conditions are less conducive. Deardorff (1976) quantified Woodcock's results, using surface-layer similarity theory to show that gull soaring flight predominates when buoyancy-driven turbulence dominates. Given the success of these studies in using soaring birds as qualitative data-gathering platforms, the newly developed technology for instrumenting these birds with the appropriate sensors suggests that they could also be used to gather quantitative information on boundary-layer meteorological processes.

The present study applies this newly proposed thermal updraft sampling technique to explore the differences in thermal updraft intensity observed over a broad flat-floored valley and adjacent mountain ranges. A summary of the required boundary-layer dynamics and avian aerodynamics is presented in Section 2. These meteorological and aeronautical similarity theories are combined to calculate thermal updraft intensity from the climb rates of soaring birds circling

within thermal updrafts. A simple diagnostic boundary-layer model is developed to model inter-day and diurnal variations in the boundary-layer depth and convective velocity scale, as described in Section 3. Model-produced estimates of these boundary-layer meteorological parameters are used with mixed-layer similarity theory to normalize measurements of thermal updraft intensity obtained from American white pelicans (*Pelecanus erythrorhynchos*) soaring over complex terrain. The data gathered and methodologies employed during this study are described in Section 4. The vertical profiles of normalized averaged thermal updraft intensity over the valley and the nearby mountains are computed. In Section 5, these plots are compared with and contrasted to each other, as well as to related results obtained in previous studies.

2. Theory

2.1. Convective boundary-layer dynamics

Several studies have examined the vertical profile of thermal updraft intensity, although interpretation of the results is complicated by various researchers' use of different thresholds to define thermal updrafts and downdrafts (Schumann and Moeng, 1991). For example, in examining a time series of vertical velocity data obtained from aircraft measurements, Young (1988) defined those parts of the data series with positive vertical velocities as thermal updrafts, while the remainder of the data series was classified as environmental downdraft. Young showed that the mean vertical velocity in thermal updrafts $\overline{w_T}$ at some altitude z can be approximated through the relationship,

$$\frac{\overline{w_T}}{w_*} = 0.85 \left(\frac{z}{z_i}\right)^{1/3} \left(1.3 - \frac{z}{z_i}\right), \tag{1}$$

where z_i is the boundary-layer depth and w_* is the convective velocity scale (Deardorff, 1970), defined as,

$$w_* = \left(\frac{g z_i B}{\bar{\theta}_v}\right)^{1/3}. \tag{2}$$

Here g is the gravitational acceleration, $\bar{\theta}_v$ is the mean boundary-layer potential temperature, and B is the surface virtual potential temperature flux. Using aircraft data from a different study, Greenhut and Khalsa (1982) defined thermal updrafts and downdrafts as those parts of the data series that exceed a specific velocity threshold. Thermal updrafts are defined as that part of the data series in which the vertical velocity exceeds $0.56w_*$, and thermal downdrafts are defined as that part of the data series in which the vertical velocity is less than $-0.40w_*$. These criteria are more stringent than those of Young (1988) so Greenhut and Khalsa (1987, Figure

5) found that the maximum value of the vertical profile of normalized average vertical velocity ($w/w_* = 1.16$) is markedly greater than that ($w/w_* = 0.56$) found by Young (1988, Figure 4). The values differ because Young averages over all measured positive vertical velocities in his time series, whereas Greenhut and Khalsa only average over those portions of the measured positive vertical velocities in their time series that exceed the predefined cutoff value. Schumann and Moeng (1991) demonstrated that the results obtained in both of these observational studies are replicable by applying their respective criteria to the same LES data set. Given the success of Greenhut and Khalsa, Young, and Schumann and Moeng in developing mixed-layer similarity formulae for thermal updraft intensity, results from these studies are used as baselines for comparison with the thermal updraft intensity measurements obtained during the present study.

The mixed-layer similarity formulae described above show that estimates of thermal updraft intensity are influenced by two key boundary-layer parameters: the boundary-layer depth z_i and the convective velocity scale w_*. Although measurements of the boundary-layer depth and the convective velocity scale are preferred when studying thermal updraft intensity, such measurements are often difficult to obtain by direct observation except at widely separated locations. As a result, estimates of the boundary-layer depth and convective velocity scale are often obtained through numerical modelling. A simple boundary-layer forecast model is developed here to diagnose changes in these parameters during this study. These data are then used to normalize, via mixed-layer similarity, the measurements of thermal updraft intensity obtained by calculating the climb rates of birds soaring in thermals. Given that avian soaring performance is also influenced by such factors as the morphological characteristics and flight objectives of these birds, an understanding of avian aerodynamics is necessary to measure thermal updraft intensity via this approach.

2.2. AVIAN AERODYNAMICS

Avian soaring performance is typically expressed as the relationship between the sink rate V_z of a gliding bird and the bird's forward flight speed V in straight flight. The soaring performance of a given species can be determined by fitting a curve to measured values of forward flight speeds and corresponding sink rates. Employing this approach, Pennycuick (1971) derived a performance curve for White-backed vultures (*Gyps africanus*) based upon 94 measurements of vulture flight speeds and sink rates.

Welch et al. (1977) theorized that gliding birds, being governed by the same physics, obey the same aeronautical performance equation as gliding aircraft,

$$V_z = \frac{2kW}{\pi\rho b^2 V} + \frac{C_{Do}\rho S V^3}{2W}, \tag{3}$$

where W is the weight of the bird, ρ is the air density, b is the wing span, S is the wing area, and k and C_{Do} are species-dependent aerodynamic drag coefficients.

Pennycuick et al. (1998) terms the drag coefficient k the induced drag factor that measures the efficiency of the wings in producing lift. A value of unity represents a perfectly efficient wing, where as increasingly higher values are representative of increasingly inefficient wings. Pennycuick describes the drag coefficient C_{Do} as a measure of the degree to which the body of a bird is streamlined. The lower the value of C_{Do}, the greater the degree to which the body is streamlined. Typical values of k and C_{Do}, as determined from wind-tunnel studies and theoretical expectations for these coefficients, are 1.1 and 0.1 respectively for many species of birds. Pennycuick (1971) derives a second performance curve for White-backed vultures by solving (3) using measured values of the weight, wing span, and aspect ratio (i.e., ratio of wing span to width) for this species, and assuming representative values for the drag coefficients. His comparison of these two curves shows that they are statistically indistinguishable, and thus, that a good estimate of avian soaring performance can be obtained via (3) and bird morphological characteristics.

The sink rate of a circling bird can be related to the sink rate of the same bird in straight, gliding flight through the expression

$$V_{zc} = \frac{V_z}{\sqrt{(\cos^3 \phi)}}, \tag{4}$$

where V_{zc} is the sink rate of a soaring bird circling at a bank angle ϕ (Haubenhofer, 1964). Pennycuick (1971, 1998) notes, moreover, that the decrease in the density of air with altitude causes an increase in the sink rate of a soaring bird circling in still air. This density-corrected sink rate may be computed via

$$V_s = V_{zc}\sqrt{\frac{\rho_o}{\rho}}, \tag{5}$$

where ρ and ρ_o are the densities of air at the flight altitude and the mean sea level (MSL), respectively. This relationship is used to obtain a more precise estimate of a bird's sink rate at various heights within the boundary layer.

The climb rate V_c for a soaring bird is related to its sink rate V_s through an ascending thermal,

$$V_c = w - V_s, \tag{6}$$

where w is updraft intensity averaged around the bird's circular flight path. Solving (6) for w allows an estimate of thermal updraft intensity to be obtained by measuring the climb rate of a soaring bird circling in a thermal updraft, and using Equations (3), (4), and (5) to estimate the sink rate of this bird from its morphological characteristics. Glider pilots often use these relationships to diagnose vertical air motions based upon the observed climb rate of the glider and the aerodynamic characteristics of this glider (Reichmann, 1993). Unlike fixed-wing aircraft, however, birds have the capability of altering their wing spans, and thus

wing areas, during the course of a flight, thereby changing their sink rates relative to still air. Because changes in these bird flight parameters, including wing area and forward speed, can significantly influence the calculation of thermal updraft intensity, knowledge of bird behavioural patterns is necessary to estimate the soaring performance of these birds within thermal updrafts.

Soaring birds are often observed circling and gliding at low-levels while searching for food or maintaining a home range (e.g., patrolling the airspace surrounding a nest). Although birds engaged in such flight will often use thermals to maintain or gain altitude, these birds do not need to maximize their climb rate in thermal updrafts to accomplish their flight objectives. As a result, the flight speed, wing area, and hence sink rate of the birds relative to still air cannot be assumed to take on their optimal values.

In contrast, cross-country soaring offers a much more workable alternative because performance optimization does benefit birds in this flight mode. Thermal cross-country soaring is often simulated using the discrete thermal model discussed by Welch et al. (1977), Pennycuick (1972, 1975), and others. This theoretical model assumes that soaring birds gain altitude by circling in thermals, and then lose altitude while gliding cross-country between thermals, behaviour generally observed by others (Pennycuick, 1971a) and in our observations of soaring American white pelicans. The primary flight objective of birds engaged in such flight is to fly from one location to another. Thus, the theories of avian cross-country soaring flight suggest that birds should optimize soaring performance to maximize their cross-country flight speeds. The cross-country speed V_{cc} of a soaring bird may be approximated by

$$V_{cc} = \frac{d_x}{t_x + t_t}, \tag{7}$$

where d_x is the horizontal distance travelled between two thermals, t_x is the time spent gliding between these thermals, and t_t is the time spent climbing in one thermal (Reichmann, 1993). Given that the time spent in thermal updrafts can significantly influence this flight speed, it is reasonable to assume that birds circling in thermals will minimize their sink rate relative to still air to maximize their climb rates within thermal updrafts. An estimate of the minimum sink rate for a species may be found by using averaged values of the weight, wing span, and wing area for a species to find the global minimum of V_z in (3). This minimum sink rate occurs at a specific forward speed for each species and requires that birds extend their wings to full wing span (Pennycuick, 1975).

Significantly, this conceptual model of avian cross-country soaring flight suggests that birds should soar to relatively high altitudes within the boundary layer to maximize their cross-country flight speed. This strategy enables birds to glide longer distances between thermal updrafts, thereby increasing their chances of finding the next soarable thermal without having to flap as they sink closer to the ground. Furthermore, by flying through the middle of the boundary layer, these

birds stay within that portion of the boundary layer where thermal updraft intensity is typically the greatest (Schumann and Moeng, 1991). For these reasons, it is advantageous for birds soaring cross country to confine the majority of this flight to the middle of the boundary layer. Observations discussed below show that soaring American white pelicans do indeed follow this approach.

3. Model Characteristics

3.1. Model architecture and data

A numerical model has been created to diagnose the daily development and evolution of boundary-layer depth and thermal updraft intensity. This one-dimensional column model simulates changes in these parameters to a maximum altitude of 4000 m above ground level (AGL). Three key data sets are required to initialize and force this model. The first two data sets, required for model initialization and forcing respectively, are atmospheric sounding and hourly surface air temperature and pressure data. These data sets combined are used to diagnose inter-day and diurnal changes in boundary-layer depth by applying the simple parcel-lifting technique illustrated in Figure 11.11 of Stull (1988). The boundary-layer depth is specified as the height above ground level at which a parcel of air rising from the surface layer and conserving potential temperature becomes negatively buoyant relative to the ambient environment. Surface air temperature and pressure data, obtained from a height of 3 m AGL, are used in this model so as to approximate the vertical extent of the most buoyant (i.e., least diluted by lateral entrainment) thermals within the boundary layer (Crum et al., 1987). Given the definition of boundary-layer depth provided above, these data help identify the depth within which all but the very strongest thermals within the boundary layer will extend.

The final data set, also required for model forcing, is upper-air forecast data from a large-scale atmospheric model. Advection by synoptic-scale weather systems often causes significant inter-day and intra-day changes in the atmospheric potential temperature profile. Given that such changes significantly influence boundary-layer depth and thermal updraft intensity (Stull, 1988), advective changes in the boundary-layer model potential temperature profile must be included throughout this model run. The NWS Early-Eta model forecast is used for this purpose. Forecast atmospheric soundings are derived from Early-Eta model output obtained at 50-hPa intervals from 1000 to 500 hPa. This vertical spacing, while sufficient to resolve the large-scale advective changes, is not sufficient for the Early-Eta forecast to be used in place of the diagnostic boundary-layer model to find the boundary-layer depth directly.

3.2. MODEL INITIALIZATION AND FORCING

The basic function of the diagnostic boundary-layer model is to simulate numerically the simple graphical method for determining boundary-layer depth illustrated in Figure 11.11 of Stull (1988). Measured 1200 UTC atmospheric sounding data are used to initialize the model atmospheric potential temperature profile. Similarly, 1800 and 0000 UTC Early-Eta model forecasts are used to describe the expected atmospheric potential temperature profile 6 h and 12 h after the boundary-layer model initialization. Hourly surface air temperature and pressure data can be input either from Early-Eta forecasts, MOS statistical guidance (Jacks et al., 1990), or surface observations. Observations from Naval Air Station (NAS) Fallon are used in this study. When found graphically, the boundary-layer depth is identified as that altitude at which the dry adiabat corresponding to the surface potential temperature intersects the vertical profile of potential temperature. In non-arid regions the virtual potential temperature should be used. The numerical model simulates this graphical technique by linearly interpolating the measured and forecast atmospheric sounding data at 1-m intervals to describe the vertical profile of potential temperature at 1200, 1800, and 0000 UTC. Temporal changes in the model potential temperature profile are then simulated by linearly interpolating at one-minute intervals between the 1200 and 1800 UTC model soundings during the first half of the model run, and between the 1800 and 0000 UTC model soundings during the latter half of this run. Corresponding changes in the surface air potential temperature are estimated each one-minute time step by applying a cubic spline to hourly values of the surface air potential temperature, as derived from the hourly surface air temperature and pressure measurements. Finally, the boundary-layer depth is estimated each minute by identifying the altitude above ground level at which the modelled surface potential temperature and the potential temperature along the vertical profile of potential temperature are equal. The resulting boundary-layer model output consists of boundary-layer depth estimates each minute between 1200 and 0000 UTC. These model estimates vary smoothly over time, suggesting that the temporal and spatial interpolation intervals applied in this model introduce little if any additional uncertainty beyond that expected when numerically simulating the simple parcel lifting technique described by Stull.

In addition to diagnosing changes in boundary-layer depth, the boundary-layer forecast model diagnoses the time series of the surface virtual potential temperature flux, approximated from hereon by the surface potential temperature flux because of the arid conditions. The boundary-layer forecast model calculates this flux at each time step by implementing a simple heat budget. This model assumes that the change in the boundary-layer potential temperature $\Delta\theta$ at each time step Δt is a function of the surface potential temperature flux B, mixing entrainment across the top of the boundary layer E, and the horizontal advection A of potential temperature such that,

$$\frac{\Delta\theta}{\Delta t} = \frac{B}{z_i} + \frac{E}{z_i} + A, \tag{8}$$

where z_i is the boundary-layer depth. Equation (8) can be rewritten to solve for the surface potential temperature flux,

$$B = \left(\frac{\Delta\theta}{\Delta t} - A\right) z_i - E. \tag{9}$$

Entrainment E represents the amount of heating that occurs within the boundary layer as a result of thermals mixing air from the free atmosphere into the boundary layer. Past studies have shown that this mixing is proportional to the surface potential temperature flux, typically varying between $-0.1\ B$ and $-0.3\ B$, especially in low-shear environments (e.g., Stull, 1976). In this study the entrainment E is approximated as $-0.2\ B$. Thus, (9) reduces to,

$$B = \frac{z_i}{1.2}\left(\frac{\Delta\theta}{\Delta t} - A\right). \tag{10}$$

Assuming that the entrainment E varies over the range of typical values, this approximation introduces an 8% error in the estimated value of the surface potential temperature flux. The change in the boundary-layer potential temperature at each time step is derived from hourly surface air temperature and pressure data, as summarized above, while the horizontal advection is derived from Early-Eta forecast sounding estimates.

Similar to the model-derived soundings described above, the vertical profiles of horizontal winds above NAS Fallon at 1200, 1800, and 0000 UTC are specified using Early-Eta model output interpolated at 1-m intervals. The vertical profiles of potential temperature at points located 80 km to the north, south, east, and west of NAS Fallon are also specified at 1200, 1800, and 0000 UTC using the same methodology. The distance between these points and NAS Fallon is consistent with the 80-km horizontal grid spacing of the Early-Eta model. A finite-differencing scheme is applied to estimate the vertical profile of the horizontal potential temperature advection above NAS Fallon at these three times. Temporal changes in the model profile of horizontal temperature advection are then simulated by linearly interpolating between the 1200 and 1800 UTC model-derived profiles during the first half of the model run, and between the 1800 and 0000 UTC model-derived profiles during the latter half of the run. These interpolations are applied each time step, and provide an estimate of the heating rate within the boundary layer due to the horizontal advection of potential temperature into this atmospheric layer. The advection and corresponding boundary-layer depth estimate are input into (10) to obtain the surface potential temperature flux B. Model output thus includes the surface potential temperature flux for each minute from 1200 to 0000 UTC. In this study, the model was used to simulate boundary-layer development and evolution

in a relatively arid environment. For this reason, the contributions of moisture to the surface virtual potential temperature flux were considered negligible, and thus the surface potential temperature flux and surface virtual potential temperature flux were assumed equal. Values of the surface potential temperature flux B are therefore used to calculate changes in the convective velocity scale w_* via Equation (2). These modelled estimates of the convective velocity scale are used to normalize measurements of thermal updraft intensity in the results presented below.

Significantly, these relationships show that, in the absence of hourly surface air temperature data, surface potential temperature flux data can be used to determine inter-day and diurnal changes in the boundary-layer potential temperature. Although surface potential temperature flux data typically are not collected at most weather observation sites worldwide, a flux forcing option has been built into this diagnostic boundary-layer model to enable its use when surface air temperature data are unavailable. Both modes of model operation, with surface observations and with model output only, are used in the results presented below to simulate inter-day and diurnal changes in the boundary-layer depth within the study area.

4. Fallon, Nevada 1997 Field Study

4.1. Goals and objectives

During June and July 1997, a field study was conducted in the Fallon, Nevada (NV) area to measure thermal updraft intensity using American white pelicans as biological UAVs. The primary goal of this study is to examine the relationship between thermal updraft intensity and model-produced estimates of the boundary-layer depth and convective velocity scale over a range of terrain elevations, and thus to determine the impact of complex terrain on the validity of thermal updraft intensity estimates derived from mixed-layer similarity theory. The first objective of this study is, therefore, to verify the accuracy of the one-dimensional boundary-layer model described above. Atmospheric data were obtained from local weather observation stations, including NAS Fallon, and through visual observations throughout this study. These data are used to initialize and force the model, and to verify model performance in the Fallon, NV area. Each type of data is used either for model initialization and forcing or for model verification, never both. The second objective of the study is to obtain estimates of thermal updraft intensity over the Lahontan valley and nearby mountains. Pelican flight time and altitude data were gathered through visual observations and through instrumentation aboard these pelicans. These data were retrieved from the pelicans' onboard sensors via satellite and conventional radio telemetry.

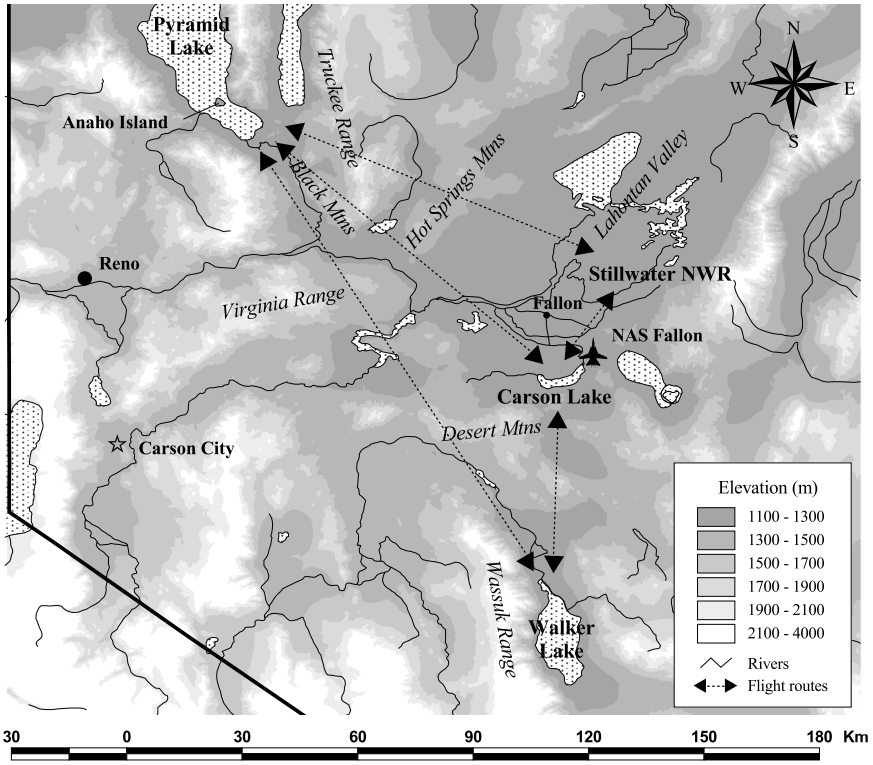

Figure 1. The pelican foraging and breeding sites and typical flight routes in the Fallon, NV area. The breeding colony is located on Anaho Island, Pyramid Lake in the northwest corner of the map. Foraging sites include Stillwater NWR, Carson Lake, and Walker Lake.

4.2. STUDY AREA AND FLIGHT PATHS

Figure 1 shows the location of known American white pelican foraging and breeding sites in the Fallon, NV area. A pelican breeding colony is located on Anaho Island, Pyramid Lake, approximately 50 km northeast of Reno, NV. Several pelican foraging sites are located between 100 and 145 km to the south and east of Anaho Island. These sites include Stillwater National Wildlife Refuge (NWR), Carson Lake, and Walker Lake. The majority of the flight altitude data obtained during this study were obtained while pelicans flew cross-country between the breeding colony and these foraging sites; the sites are located in valleys at elevations on the order of 1200 m MSL. When making data collection flights among these sites, pelicans frequently flew over mountains with peaks ranging from nearly 1700 m to over 2100 m MSL. Among the most frequently crossed mountains were the Truckee range, Hot Springs mountains, and Virginia range.

The study area was selected both because of the available flight paths and because the climatological and geographical conditions favoured development of strong thermals. Despite the abundance of water at the breeding and foraging sites

the study area as a whole is relatively arid. During June and July combined, the normal rainfall at NAS Fallon is approximately 15 mm (NOAA, 1974). Hot days and mild nights are also characteristic of this region. During this time period, the normal high and low temperatures are 31 and 10 °C respectively (NOAA, 1974). Vegetation is relatively sparse throughout the study area, and covers approximately 50% of the ground area.

4.3. BIOLOGICAL DATA

4.3.1. *Instrumentation*

Pelican-mounted sensors were used to measure the flight altitude of each pelican. Conventional and satellite radio telemetry transmitters were employed in returning these data for analysis. Each radio telemetry package consisted of a 13 g conventional radio telemetry transmitter epoxied to a 95 g satellite telemetry transmitter. The entire package was attached to the back of each pelican using a 13 g leather and teflon harness. Each satellite telemetry transmitter is equipped with a Motorola MPX4115AS temperature compensated and calibrated piezoresistive absolute pressure transducer to measure bird flight altitudes. The data sampling rate was approximately one measurement every 60 s. Thus, measurements from these transmitters provided a detailed description of bird flight altitudes, at a frequency such that bird climb rates could be determined at a relatively high vertical resolution, even when bird flight altitudes were changing rapidly. Message monitors (i.e., satellite uplink receivers) were used to obtain altitude data directly from the pelicans via their satellite telemetry transmitters. These data were transmitted in a hexadecimal format, and were archived in laptop computers attached to the message monitors. Conversion equations were supplied with the transmitters to convert the raw hexadecimal data to altitude data during post-study analysis. Each satellite telemetry transmitter was tested to verify the accuracy of these altitude data prior to attaching these transmitters to pelicans.

4.3.2. *Evaluation of Altitude Sensor Performance*

On 6 May 1997, five satellite telemetry transmitters were placed in the unpressurized cabin of a Cessna 210 and flown to a broad range of altitudes. During each horizontal flight segment, altitude readings from these transmitters were recorded, as were altitude measurements from both the altimeter of the aircraft and a control altimeter housed within the cabin of the aircraft. The nominal altitudes at which the aircraft was held level were 1520 m, 1830 m, 2130 m, 2440 m, 2740 m, and 3050 m MSL. After the flight, the raw hexadecimal data were converted to altitude using the manufacturer's conversion equations. Data from each horizontal flight segment were then analyzed to assess transmitter altitude sensor accuracy. Atmospheric turbulence caused slight deviations (i.e., estimated ± 30 m) in the altitude of the aircraft during each horizontal flight segment. Therefore, an average control altimeter reading for each segment is used to approximate the actual altitude of the

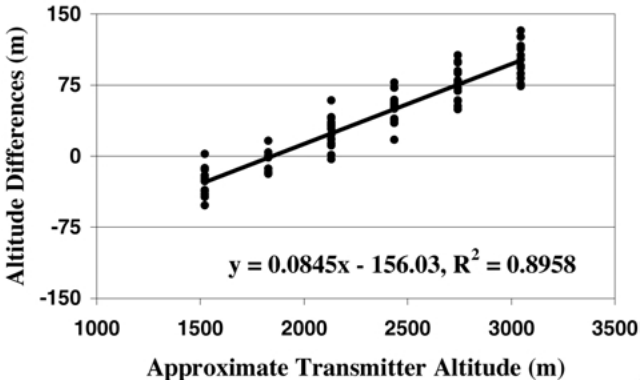

Figure 2. The differences (dots) between the transmitter-derived altitudes and the control altimeter-derived altitudes for each horizontal flight segment. The approximate altitudes are based on data obtained from the control altimeter within the aircraft.

transmitters. Although control altimeter readings closely parallel those observed on the aircraft altimeter, control altimeter readings average approximately 20 m higher than those recorded on the plane's altimeter. The 95% confidence interval for this mean μ is determined to be ± 3 m based upon a one-sample t-test. Given that the differences in these readings are relatively insensitive to height over the range of flight altitudes (i.e., 1530 m), these differences are attributed to the dynamic pressure field caused by the flow around the aircraft, as opposed to significant calibration differences between these instruments. Because the control altimeter was within the aircraft during this flight, as were the transmitters being tested, control altimeter data are used to verify transmitter sensor performance.

The difference between each transmitter-derived altitude measurement and the control altimeter data was computed for each horizontal flight segment. These differences were then plotted as a function of the control altimeter data to evaluate the performance of these sensors, as shown in Figure 2. The differences between transmitter-derived and control-altimeter derived altitude measurements increased with height. This increase is approximately linear. This linear bias suggests that differences between the control altimeter readings and the transmitter-derived altimeter readings are a result of calibration differences between the two types of instruments. Transmitter-specific linear correction equations were developed to remove this bias in the processed telemetry data. The standard deviations σ in the differences during each horizontal flight segment, with this bias removed, ranged from 12 to 18 m. This remaining scatter is primarily attributed to the slight deviations in the altitude of the aircraft during each horizontal flight segment. A similar test flight was conducted on 3 June 1997 to test the remaining five satellite telemetry transmitters. Nearly identical results were noted. Transmitter-specific linear correction equations were developed for each of these transmitters as well.

4.3.3. *Methodology*

Ten American white pelicans were instrumented with altimeter-equipped radio telemetry packages during this study. Five pelicans were captured and instrumented at Anaho Island, Pyramid Lake on 6 May 1997. An additional five pelicans were captured and instrumented at Stillwater NWR on 8 June 1997. Morphological measurements were obtained from each bird to estimate the soaring performance of this species, and in particular that of the individuals to be studied. Among the measurements recorded were the weight, half-wing span, and body girth of each bird. Additionally, one wing from each bird was traced to estimate the wing area. These bird morphological data were provided to Dr. Colin Pennycuick, who developed a glide polar for this species based upon the avian aerodynamic theories discussed above. Finally, prior to each bird's release, the head and neck of each individual were coated with a yellow dye (i.e., picric acid) to help researchers identify radio-marked pelicans during this study. Daily tracking of these birds commenced on 9 June 1997.

Two two-person teams were deployed daily to obtain pelican flight altitude, behavioural, and location data. The primary task of each team was to obtain pelican flight altitude data from radio-marked birds as they flew among foraging and breeding sites. Conventional radio telemetry transmissions were monitored to locate and home in on the instrumented pelicans. Once the team was close enough, message monitors were used to receive bird flight altitude data via the satellite telemetry transmitters. Pelican tracking was accomplished using a car or light aircraft; approximately 80 hours of aerial tracking was accomplished using a Cessna 172. Individual birds were tracked either until the bird landed, radio contact was lost, or the vehicles were forced to refuel. Although ground-based observers could obtain accurate bird flight altitude data, precise bird behavioural and location data were often difficult to obtain from the ground. As a result, the majority of these behavioural and location data was obtained during aerial tracking when the individual or flock containing the individual could be monitored visually. Such observations were critical in identifying the location of soaring birds relative to terrain, and in documenting bird behavioural patterns relative to other individuals within flocks.

Care was taken to observe the birds from extreme binocular range and from as much altitude differential as possible so as not to disrupt their flight behaviour. Moreover, observations of soaring pelicans obtained during this study suggested that these transmitters had little effect on pelican flight and behavioural patterns. Instrumented pelicans were often observed soaring in flocks ranging in size from a few birds to several hundred birds. During extended glides, radio-marked birds were observed near the leading edge of the V-shaped patterns, as well as near the trailing edge of these patterns. Furthermore, radio-marked pelicans maintained their position within the V-shaped patterns throughout any one gliding bout. Similarly, radio-marked pelicans were often observed climbing at the same rate as the other birds within soaring flocks. Given the similarities in the observed flight and behavioural patterns among instrumented and non-instrumented pelicans, we

concluded that these transmitters had little effect on the soaring performance or behaviour of the instrumented pelicans.

4.3.4. *Data Processing and Quality Control*

Altitude data are divided into temporal blocks to facilitate quality controlling. Each block consists of data obtained from one bird, where no more than 60 minutes had passed between altitude readings. The data pattern in each block is examined to identify erroneous data points. The primary indicator of erroneous altitude measurements is inconsistencies in the transmitter counter data pattern. Each satellite telemetry transmitter was equipped with a counter, designed to increment by one for each telemetry transmission. These counter data were transmitted along with altitude data. During this study, discontinuities in the counter data pattern (e.g., 40, 41, 42, 93, 44, 45) are noted when weak signals were received from the satellite telemetry transmitters. Given that altitude data obtained when signal strength was weak are often not reliable, the altitude measurement corresponding with a discontinuity in the counter data pattern is removed to maintain consistency in the data set. Blocks of data consisting of less than three altitude measurements are discarded because it is impossible to evaluate the counter data pattern using only two data points. Finally, a few measurements indicating pelican climb rates in excess of 10 m s^{-1} are discarded because such climb rates are not achievable within purely thermal updrafts. Quality controlled pelican flight altitude data are then converted to metres AGL, taking into account variations in the terrain elevations within the study area.

4.3.5. *Terrain Height Estimates*

The depth of the boundary layer often varies with changes in the elevation of the Earth's surface (Arritt et al., 1992; Banta, 1984). Model-produced estimates of this depth were calculated relative to ground-level elevation because of this terrain dependency. In contrast, measurements of pelican flight altitudes were initially calculated relative to MSL because the transmitter altimeters were calibrated relative to MSL by the manufacturer. Given the intimate relationship between soaring pelicans and boundary-layer meteorological processes, these data were recalculated relative to ground-level elevation to determine bird flight altitudes relative to boundary-layer depth. These terrain-dependent, normalized data were then used to measure thermal updraft intensity, and to determine what effects changes in terrain elevation have on these intensities.

Figure 1 shows that significant variations in terrain elevation exist within the study area. The precise location (i.e., latitude and longitude) of each bird altitude measurement was, however, typically not available. Thus, pelican altitude data were divided into terrain elevation groups based upon observed pelican locations relative to known terrain features. An approximate average elevation was assigned to each geographical region within the study area that exhibited relatively homogenous elevations. The elevation of each geographical region was then used to

calculate bird flight altitudes relative to ground level, and to specify the elevation of the Earth's surface within the boundary-layer model. Four elevation groups were designated based upon these criteria. These groups are designated as the Lahontan valley, small mountains, large mountains, and other valleys.

Most pelican foraging sites within the Lahontan valley were located in the Fallon, NV area. Instrumented pelicans typically foraged in Carson Lake and smaller bodies of water within the Stillwater NWR. The approximate elevation of these sites was 1190 m MSL with little variation. Most pelicans departing these foraging sites flew west or northwest towards the Hot Springs mountains. The terrain flown over generally ranged in elevation from 1190 m to 1210 m MSL, gradually increasing as the birds flew closer to the mountains. Based upon these values, the average elevation of the Lahontan valley was approximated as 1200 m MSL.

Several of the mountain ranges within the study area are relatively similar to one another in elevation. For example, the Hot Springs mountains, eastern Virginia range, and Black mountains are all characterized by peaks approaching 1700 m MSL, with the bases of these mountains ranging in elevation from about 1200 m to 1250 m MSL. Jagged orography resulted in much fluctuation of height across this range within each group of mountains. Mountains exhibiting these characteristics were designated as small mountains, and assigned an average elevation of 1460 m MSL. Similarly, those parts of the larger mountains within the study area where the elevation varied between approximately 1200 m and 1700 m MSL were considered small mountains. Pelicans occasionally crossed mountains within the study area that contained peaks approaching or exceeding 2000 m MSL. These mountains included portions of the Truckee range, the Desert mountains, and the Wassuk range. Those parts of these mountains where the elevation exceeded 1700 m MSL were characterized as large mountains. The average elevation for large mountains was approximated as 1850 m MSL. The remaining unclassified regions within the study area consisted of those lowlands within the study area other than the Lahontan valley. Examples of these lowlands included several river valleys in the western portion of the study area, as well as the lowlands surrounding and immediately adjacent to Pyramid Lake and Walker Lake. Similar to the Lahontan valley, the average elevation of the other valleys was approximated as 1200 m MSL.

The error introduced by uncertainties in terrain elevation is small compared to the modelled estimates of boundary-layer depth obtained during this study. Because we are assuming an average elevation for each terrain group, the maximum error in elevation is one-half the range of values in each group. Therefore, this error is approximately 250 m over the mountains and about 10 m over the valleys. Boundary-layer depth estimates corresponding to the times that bird flight altitude measurements were obtained during this study are 2220 m ($\sigma = \pm 640$ m) over the mountains and 1520 m ($\sigma = \pm 1050$ m) over the valleys. These values suggest that the resulting uncertainty in bird flight altitudes normalized by boundary-layer depth is approximately 11% over the mountains and less than 1% over the valleys.

4.4. METEOROLOGICAL DATA

The meteorological data sets gathered during this study were used to initialize and force the boundary-layer meteorological model introduced above and to assess model accuracy in forecasting the boundary-layer depth. Additionally, these model estimates were compared with observations and measurements of pelican flight altitudes to further evaluate model performance. Finally, model output was used in conjunction with measurements of pelican climb rates to develop normalized profiles of thermal updraft intensity within the study area.

Atmospheric sounding data and hourly aviation weather reports were obtained from NAS Fallon. Weather balloons were launched at 1200 and 2100 UTC to measure the vertical profile of potential temperature within the study area; 1200 UTC balloons were launched more frequently (i.e., on more days), however, than were 2100 UTC balloons. Data obtained from the 1200 UTC atmospheric soundings were used to initialize the boundary-layer meteorological model, while data obtained from the 2100 UTC soundings were used to verify model performance. Although 2100 UTC data are useful in diagnosing changes in boundary-layer depth, these data were only used to assess model performance, thereby maintaining consistency in the method by which boundary-layer depth was calculated throughout this study. Hourly aviation weather reports were obtained to document changes in the observed surface air temperature and pressure, and hence boundary-layer potential temperature. Finally, hourly observations of precipitation, cloud type, and cloud coverage were made by each observation team to supplement these data. These auxiliary observations were necessary to identify those time periods when boundary-layer processes were dominated by thermals, and those time periods when processes other than thermals may have influenced the temporal and spatial extent of avian soaring flight. Given that the boundary-layer model described herein only simulates thermally driven boundary-layer processes, these observations were critical in determining the applicability of this model under various observed atmospheric conditions.

5. Results

5.1. ANALYSIS OF BOUNDARY-LAYER MODEL ACCURACY

5.1.1. *Disturbed and Undisturbed Period Criteria*

Boundary-layer model performance was examined by comparing diagnosed boundary-layer depths with measured boundary-layer depths at 2100 UTC. Atmospheric sounding data were obtained at 1200 UTC on 26 days during this study. On 14 of these days, atmospheric sounding data were gathered at 2100 UTC as well, and on 3 of these 14 days, precipitation was observed in the study area between 1200 and 2100 UTC. Because this simple boundary-layer meteorological model does not simulate those processes associated with the development

of precipitation, the model accuracy was examined only for the days when dry convective processes (i.e., thermals) dominated boundary-layer development and evolution between 1200 and 2100 UTC. Likewise, data analysis using this model was undertaken only for undisturbed periods, defined as follows:

undisturbed periods: those times between 1200 UTC and 1 hour before the onset of precipitation within the study area, and

disturbed periods: those times between 1 hour before the onset of precipitation within the study area, and 0000 UTC.

5.1.2. *Evaluation of Diagnosed Boundary-layer Depths*

Figure 3 presents the observed and modelled boundary-layer depths at 2100 UTC for the 11 days when undisturbed conditions prevailed between 1200 and 2100 UTC. On average, model forecasts of boundary-layer depth were slightly greater than sounding-derived measurements of this variable, exhibiting a mean positive bias of 66 m ($\pm$163 m based upon a one-sample t-test assuming 95% confidence). Significantly, these bias and uncertainty values are small relative to the mean measured boundary-layer depths for these 11 days (μ = 2400 m, σ = $\pm$640 m). Moreover, model forecasts captured most of the observed inter-day variability in boundary-layer depth (r^2 = 0.86), despite significant inter-day changes in this depth.

Comparison of the modelled and measured boundary-layer depths at 2100 UTC demonstrate model accuracy in estimating this depth during the early afternoon hours local time. Because verification data are not available between 1200 and 2100 UTC, the question remains how accurate the model is between these two times. It is reasonable to assume that the boundary-layer model is relatively accurate shortly after 1200 UTC when model estimates of boundary-layer depth are most heavily influenced by the observational data used to initialize this model. A slow decline in model performance is likely, however, as the modelled vertical profile of potential temperature becomes more representative of the Eta-forecast model soundings over time. A significant decrease in model performance is possible about mid-morning local time when boundary-layer depth typically increases most rapidly. Finally, a gradual increase in model performance is expected from late morning local time through 2100 UTC as the depth of the boundary layer begins to stabilize. Measured pelican flight altitudes are compared to modelled estimates of boundary-layer depth to further examine model accuracy.

5.2. Analysis of pelican flight altitudes

5.2.1. *Lahontan Valley*

The temporal distribution of pelican flight altitudes z normalized by boundary-layer depth z_i for all pelicans soaring over the Lahontan valley during undisturbed conditions is shown in Figure 4. Pelican flight altitudes should not exceed the

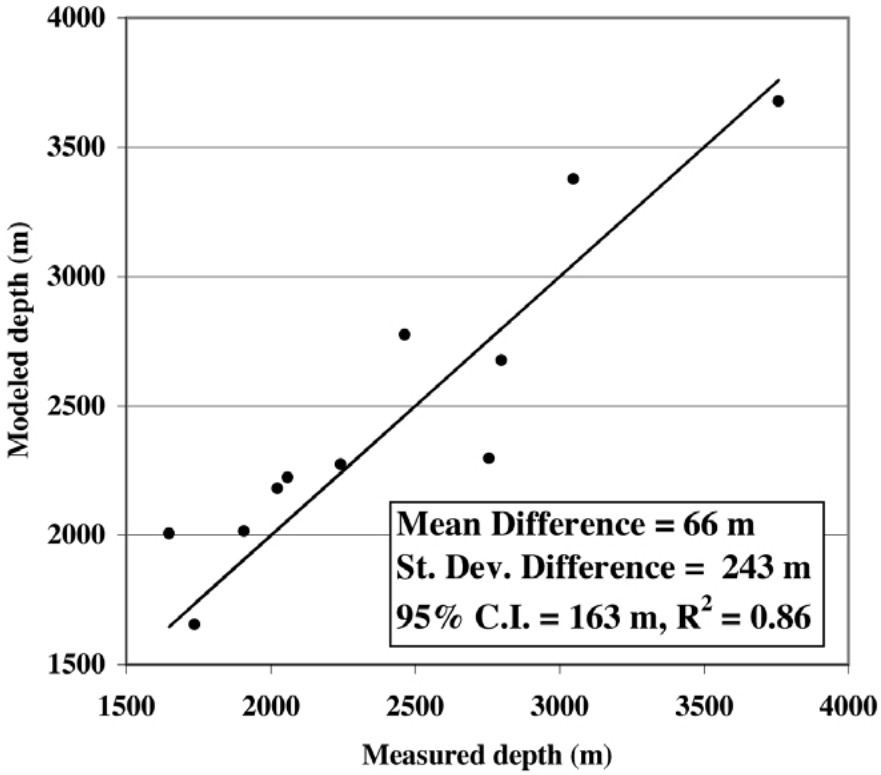

Figure 3. The measured (sounding-derived) versus modelled 2100 UTC boundary-layer depths (dots) on the 11 days that afternoon sounding data were available at NAS Fallon. The line indicates where the dots should fall on the graph if the modelled and measured depths are identical.

boundary-layer depth in an environment where thermal updrafts are the primary source of lift, however, about 11% (115 of 1003) of these points exceed $1.0z/z_i$. Assuming, based upon the verification data presented above, that model diagnoses of the boundary-layer depth average 66 m too high, and that the random error in forecasting this depth is 163 m, measured bird flight altitudes should not exceed the boundary-layer depth by more than 97 m. Approximately 31% (36 of 115) of the original data points in excess of $1.0z/z_i$ fell below this threshold when model bias and random error were factored into this analysis. While 30% of the original normalized bird flight altitudes in excess of $1.0z/z_i$ also exceeded $2.0z/z_i$, only 9% of these normalized bird flight altitudes exceeded this threshold when the model bias and uncertainty were included in this analysis. Moreover, of the 115 instances in which bird flight altitudes exceeded the forecasted boundary-layer depth, all occurred when this depth was less than 1494 m AGL, and 78% occurred when this depth was less than 609 m AGL. These analyses combine to suggest that normalized bird flight altitudes in excess of $1.0z/z_i$ are primarily a result of model errors when modelling a shallow boundary layer. This result occurs because, when

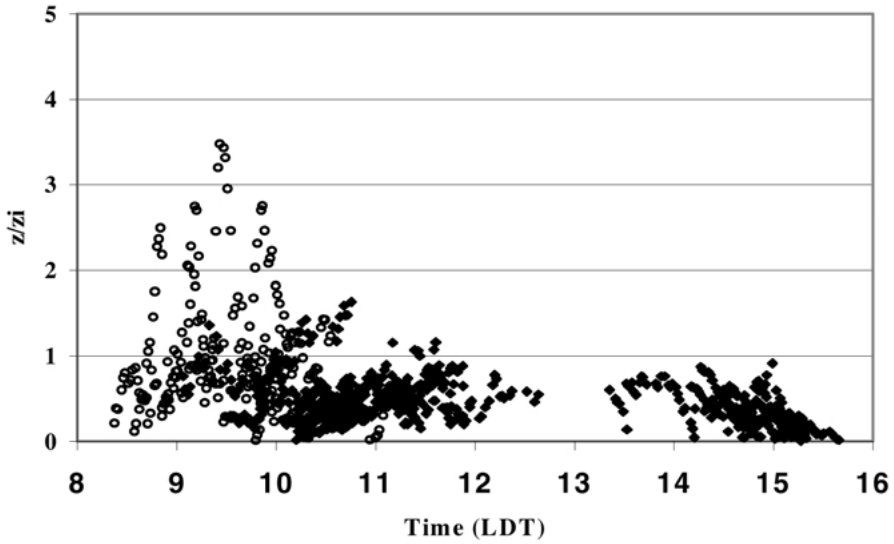

Figure 4. Temporal distribution of normalized pelican flight altitudes over the Lahontan valley for cross-country flights. Hollow circles identify those flight altitudes when the modelled boundary-layer depth was less than 609 m, while filled diamonds identify those flight altitudes corresponding to a deeper boundary layer.

the boundary layer is shallow, large errors in the normalized bird flight altitudes will arise when these altitudes exceed modelled boundary-layer depths by even a nominal margin. Indeed, 83% of the normalized pelican flight altitudes in excess of $1.0z/z_i$ occurred before 1100 LDT. These results also underscore the likelihood that soaring pelicans are selecting to use only the most intense thermal updrafts early in the development of a well-mixed boundary layer. This behaviour is necessary because, although thermals are present, not all thermals are sufficiently intense to support soaring flight. The boundary-layer model output is representative of the average thermal depth in the boundary layer, and hence may underestimate the actual depth of the thermals that birds are soaring upon early in the time period. Given these expectations and the supporting statistics, model-produced estimates of the boundary-layer depth and the surface potential temperature flux were used to normalize observed thermal updraft intensity.

The distribution of pelican flight altitudes z normalized by the diagnosed boundary-layer depth z_i for those days when 2100 UTC atmospheric sounding data were available at NAS Fallon is shown in Figure 5. These data correspond to those days when model accuracy in simulating boundary-layer depth had been verified. On these days, 85% (560 of 658) of the normalized pelican flight altitudes fell below $1.0z/z_i$. Figure 6 depicts the distribution of pelican flight altitudes z normalized by boundary-layer depth z_i for those days when 2100 UTC atmospheric sounding data were not available. On these days, 95% (328 of 345) of the data points fell below $1.0z/z_i$, supporting the results obtained when boundary-layer depth had

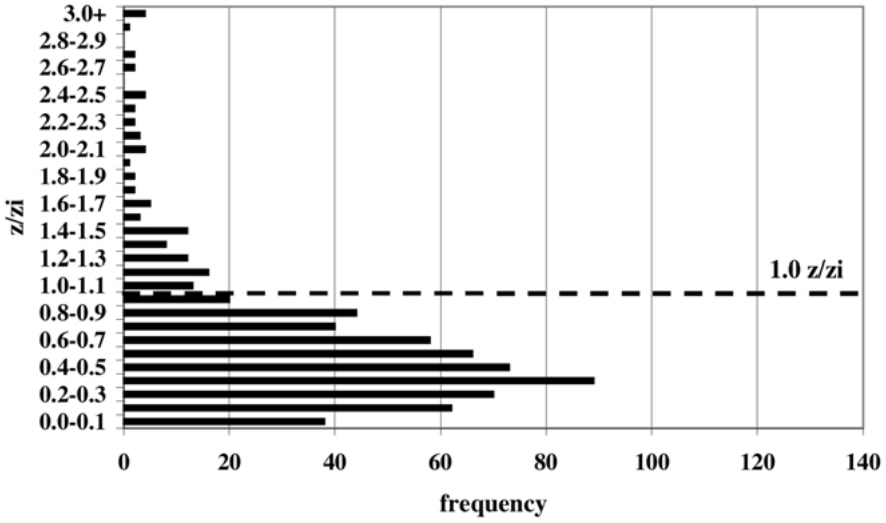

Figure 5. Distribution of normalized pelican flight altitudes over the Lahontan valley on days when 2100 UTC atmospheric sounding data were available.

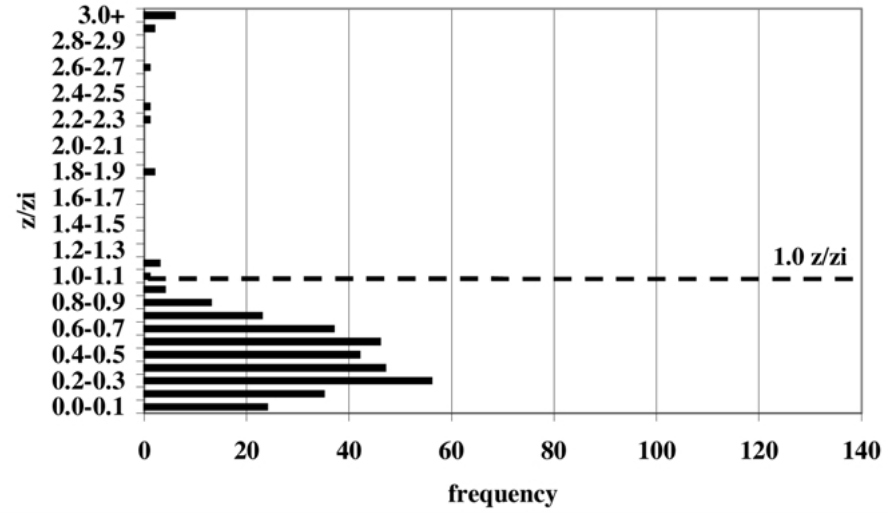

Figure 6. Distribution of normalized pelican flight altitudes over the Lahontan valley on days when 2100 UTC atmospheric sounding data were not available.

been verified. Given that pelican flight altitudes should not exceed boundary-layer depth in an environment where thermal updrafts are the primary source of lift, data from these two comparisons illustrate model accuracy in forecasting this depth. Because of the similarities between these two data sets, they were combined in all subsequent analyses.

We observed that pelican flight altitudes often vary depending on flight objectives. Changes in these flight objectives can influence the extent to which pelicans attempt to maximize cross-country soaring performance, and thus can affect how well pelican climb rates represent the actual thermal updraft intensity. Therefore, knowledge of pelican flight objectives is necessary when using pelicans as UAVs to estimate updraft intensity. Pelican altitude data were divided into flight-type categories to identify those time periods when soaring pelicans are likely to be attempting to maximize their climb rates, and thus provide a representative sample of thermals. These categories are defined based upon the horizontal extent of each pelican flight leg originating within the Lahontan valley:

local flight: any flight in which a pelican lands at the same site from which it began soaring, never having flown more than 10 km away from the point of origin,

cross-country flight: any flight in which a pelican flies more than 10 km away from the point of origin.

Birds engaging in short soaring flights never flew more than a few kilometres away from the point of origin. In contrast, birds soaring between the foraging and breeding sites always flew distances on the order of 100 to 150 km from the point of origin. Given the significant differences in the distances travelled between these two flight modes, and the apparent differences in the flight objectives of these birds, a 10-km range limit was adequate to distinguish between local and cross-country flights.

Of the 29 flight legs identified using these criteria, 4 were categorized as local flights. The altitude distribution of these local flight data is shown in Figure 7. Approximately 57% (55 of 96) of the data points associated with these local flights were between 0.1 and $0.4z/z_i$, showing that pelicans engaged in short soaring flights predominately confine much of their flight to the lower boundary layer. Of the three instrumented pelicans responsible for the four local flights, two were identified as likely non-breeders based upon their behavioural patterns during this study. One of these birds was never observed flying more than 10 km from Carson Lake, and was typically found on the lake surface. The other likely non-breeder was also an infrequent flier, mainly found in the vicinity of Carson Lake. This bird was observed completing a cross-country flight to the breeding colony. Unlike all other instrumented birds followed to Anaho Island, however, this bird returned to the foraging site without landing at the breeding colony. Although it is possible that birds engaging in local flights may be testing thermal strength in preparation for a cross-country flight, the limited number of observations during this study precludes such a conclusion. One of the four local flights was completed by a likely breeder (i.e., a pelican that frequently flew cross country between the foraging and breeding sites). Although this bird did not fly cross-country on that particular day, another instrumented bird was observed departing the same area earlier in the

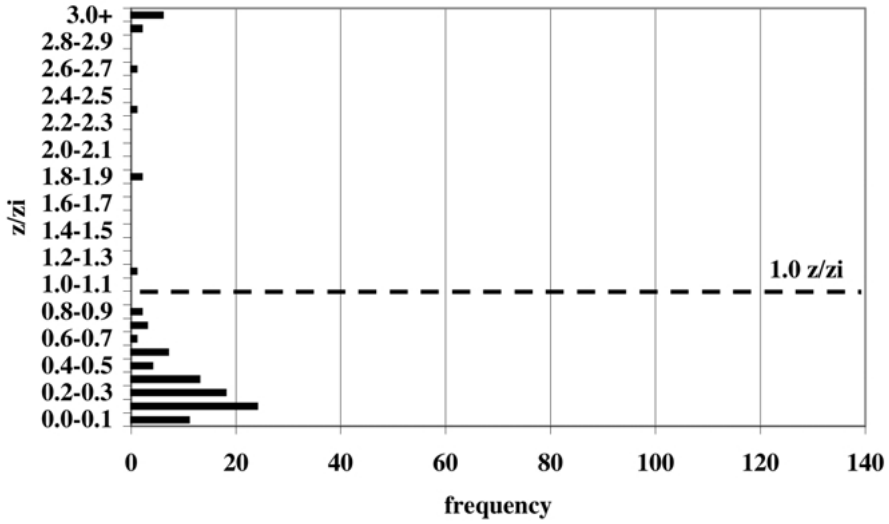

Figure 7. Distribution of normalized pelican flight altitudes for local flights.

day on a cross-country flight to the breeding colony. Therefore, these data do not support the hypothesis of birds testing thermal strength prior to a cross-country flight. Although the flight objectives of these pelicans are not definitively known, these pelicans likely remained within the lower boundary layer because they had no intention of soaring a significant distance from their foraging sites. Birds engaged in such local flights have no need to optimize cross-country soaring performance, and are therefore less likely to maximize their climb rates within thermal updrafts. As a result, local flight data were not used in analyses of thermal updraft intensity.

The remaining 25 flight legs originating in the Lahontan valley were categorized as cross-country flights. The distribution of these cross-country flight data is shown in Figure 8. In contrast to the local flight data, 60% (541 of 907) of the data points were between 0.2 and $0.7z/z_i$, confirming theoretical expectations that birds soaring extended distances should fly relatively high within the boundary layer so as to maximize their climb rates within thermal updrafts to optimize cross-country soaring performance (Pennycuick, 1975; Reichmann, 1993). Thus, only data obtained during cross-country soaring flight were used to estimate thermal updraft intensity over the Lahontan valley and the nearby mountains.

5.2.2. *Mountains*

In contrast to the situation in the Lahontan valley, atmospheric sounding and surface air temperature data were not available over the mountains. Furthermore, model estimates of boundary-layer depth over the Lahontan valley were not necessarily representative of the thermal depth over these mountains, given that boundary-layer depth often varies with changes in terrain elevation (Arritt et al., 1992; Banta, 1984). Consequently, the boundary-layer model was reconfigured for

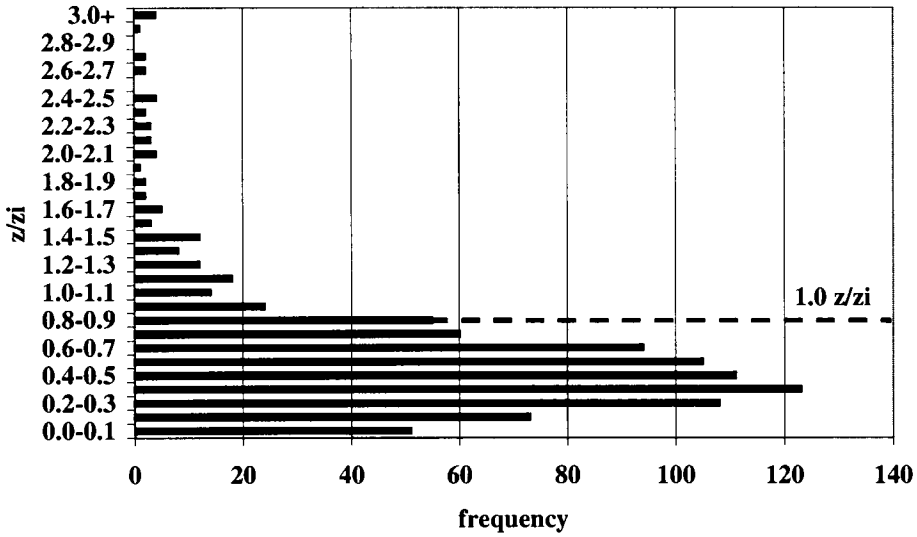

Figure 8. Distribution of normalized pelican flight altitudes for cross-country flights.

each of the terrain elevation groups specified above to simulate daily and diurnal changes in boundary-layer depth at higher elevations within the study area. Measured 1200 UTC atmospheric sounding data from NAS Fallon were modified to estimate the initial vertical profile of potential temperature over these mountains. Mountain soundings were derived by deleting all data levels between 1200 m MSL and the elevation of the specified terrain elevation group (i.e., 1460 m MSL for small mountains, 1850 m MSL for large mountains) to specify a new sounding base. This technique ignores the existence of over-mountain nocturnal inversions, an approximation considered reasonable because nocturnal drainage flows minimize the depth of such layers at mountain crests and at higher altitudes along a mountain slope (Bader and McKee, 1985). The cold air associated with these flows typically pools in the adjacent valleys below, as opposed to along the mountain slopes (Bader and McKee, 1985). These modified soundings were then used to initialize the boundary-layer model. The NWS Early-Eta model forecast soundings used to drive this model were truncated in the same manner.

Given the absence of surface air temperature data over the mountains, another method for calculating changes in the boundary-layer potential temperature was needed. Vegetation type and coverage in the study area was inspected during aerial tracking. Observations indicated that the type and coverage was similar in the valleys and the surrounding mountains. Because of the homogeneity in the ground characteristics of the Lahontan valley and the surrounding mountains, surface potential temperature flux data were expected to be similar throughout the study area (e.g., Mahfouf et al., 1987). Assuming such similarities, surface potential temperature flux estimates obtained when applying this model to the Lahontan

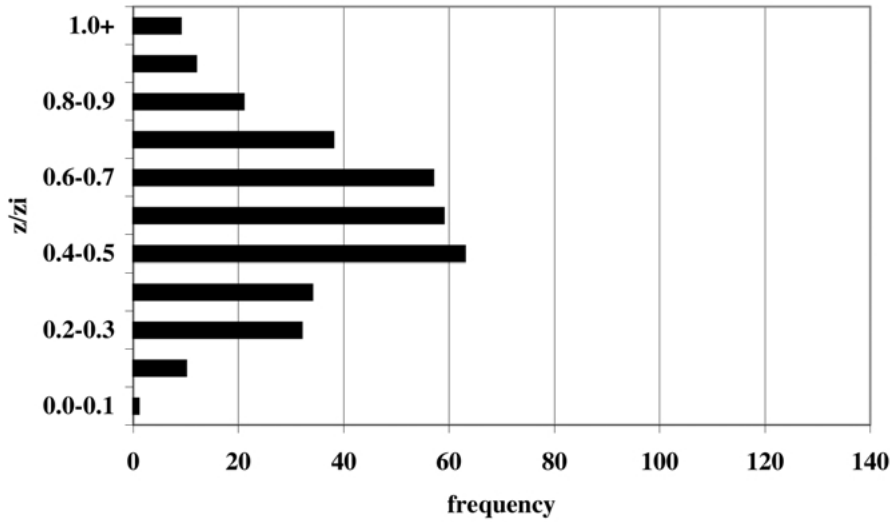

Figure 9. Distribution of normalized pelican flight altitudes over mountains.

valley were used to force this model when simulating boundary-layer development and evolution over the mountains. Thus the model used a flux boundary condition over the mountains instead of the temperature boundary condition used over the Lahontan valley.

The appropriateness of this flux boundary condition can be evaluated by the normalized pelican altitude data. The combined distribution of pelican flight altitudes z normalized by boundary-layer depth z_i for pelicans flying over higher terrain (i.e., small mountains, large mountains) is shown in Figure 9. Similar to the analysis of pelican cross-country flight altitudes over the Lahontan valley (Figure 8), 97% (327 of 336) of these normalized pelican flight altitudes were below $1.0z/z_i$, illustrating model accuracy in forecasting boundary-layer depth. Furthermore, 73% (245 of 336) of these flight altitudes were found between 0.2 and $0.7z/z_i$, showing that the majority of this type of flight was confined to the middle of the boundary layer, consistent with the theoretical expectations of avian cross-country soaring flight. Although mountain/valley circulations may have resulted in an underestimate of the model-diagnosed boundary-layer depth over the mountains, the relatively small number of flight altitudes in excess of $1.0z/z_i$ and the similarities in the preferred pelican flight altitudes over the mountains and Lahontan valley suggests that these effects were minimal. Given that all pelican data obtained over these mountains were cross-country flight data, these data were used in deriving model estimates of thermal updraft intensity over this higher terrain within the study area.

5.3. ESTIMATES OF THERMAL UPDRAFT INTENSITY

Pelican climb rates were determined by calculating the difference in the altitudes obtained from consecutive telemetry measurements and dividing by the time interval between these two measurements. Positive values were associated with birds that gained altitude, mostly by thermaling, while negative values were associated with birds that lost altitude, mostly by gliding. As a result, all negative values were discarded because such data are not useful in determining thermal updraft intensity. Furthermore, all positive climb rates in which a bird engaged in a type of flight other than thermaling between consecutive telemetry measurements were discarded. These data were typically associated with birds entering or exiting thermals during the interval between consecutive telemetry measurements, and with birds engaged in 'dolphining' flight (Reichmann, 1993) while gliding between thermals.

Equation (6) shows that thermal updraft intensity may be approximated as the sum of the measured pelican climb rate and the estimated sink rate of the same bird circling in still air. Estimates of thermal updraft intensity were obtained during this study by employing this methodology. Pennycuick (personal communication, 2001) estimated the minimum sink rate for an American white pelican in straight gliding flight at sea level as 0.61 m s^{-1} based upon (3) and the bird morphological data collected at the beginning of this study. Observations of soaring pelicans circling within thermal updrafts, obtained during aerial tracking, indicated that these birds typically flew at bank angles ϕ of about 25 degrees. Through Equation (4), the sink rate of a pelican circling in a thermal near mean sea level elevation was approximated as 0.71 m s^{-1}. Each data point was then corrected for density effects, via (5), to obtain a more accurate estimate of the pelican sink rate at that altitude.

Although pelican flight altitude data were transmitted on average every 60 s, the rate of transmissions varied. Furthermore, altitude data were not obtained every transmission because of reductions in signal strength caused by an occasional inability to point the antennae toward the birds, and because of the sometimes significant distance between the radio-marked birds and the tracking teams. As a result, a criterion was developed to specify the maximum time interval allowed between consecutive altitude measurements for thermal updraft intensity to be calculated. Only one missed transmission was allowed between two consecutive altitude measurements so as to maximize the vertical resolution of the thermal updraft data. Each estimate of thermal updraft intensity, derived from the climb rates of the thermaling pelicans, was normalized by the model-diagnosed boundary-layer depth to determine the vertical resolution of each thermal updraft intensity estimate. The median depth between successive altitude measurements was $0.07z/z_i$, indicating that on average, thermal updraft intensity data were of a relatively high vertical resolution. The resolution of these data is on the same order as the bin-averaged findings of Young (1988), who used $0.1z/z_i$ bins to examine the vertical profile of thermal updraft intensity, and had markedly better vertical resolution than the aircraft res-

ults of Greenhut and Khalsa (1987). Schumann and Moeng (1991), however, using LES, were able to achieve a better vertical resolution than all three observational studies.

Thermal updraft intensities were normalized by the convective velocity scale w_* using mixed-layer similarity. Data obtained during this experiment were grouped into equal-interval bins of $0.1z/z_i$ for comparison with previous studies. These bin-averaged data were then plotted as a function of the normalized altitude for those bins between 0.2 and $0.8z/z_i$. Data from the other bins within the boundary layer are excluded from this analysis because of the relatively small number of altitude readings available within the upper and lower boundary layer (Figure 8). Figure 10 depicts the profiles of normalized averaged thermal updraft intensity for data obtained over the Lahontan valley and the nearby mountains. Given that the minimum sink rate of an American white pelican is approximately 0.61 m s^{-1}, the portions of thermal updrafts with vertical velocities less than this value cannot be sampled using these birds because the vertical motions are too weak to support soaring flight. Thus, the normalized averaged thermal updraft intensity profiles presented here only average over those portions of updrafts having positive vertical velocities larger than a predefined cut-off value, similar to the methods of Greenhut and Khalsa (1982). The similarities between the valley and mountain profiles are apparent through visual inspection, and were confirmed through a two-sample t-test, assuming unequal variances, of the magnitudes of these profiles. For this test $P = 0.96$, and a value of P smaller than 0.05 would have been required to reject the hypothesis of equal means. Given the statistical similarity between these two profiles, these data were combined for a comparison with the thermal updraft intensity measurements obtained in previous studies.

Schumann and Moeng (1991) showed that the mixed-layer similarity profiles for thermal updraft intensity obtained using large aircraft and LES are comparable when the criteria used to define thermal updrafts in the LES are matched to those used in individual observational studies. For example, when Schumann and Moeng applied Young's criteria to their LES-produced vertical velocity field, the normalized averaged vertical velocity profiles correspond closely (Schumann and Moeng, 1991, Figure 3). Young's criteria are not applicable to the data gathered in this study, however, because the sink rate of a soaring pelican circling in still air is greater than the minimum updraft strength specified by Young. Thus, the weakest thermals cannot be resolved when applying these criteria to pelican climb rate data.

The Greenhut and Khalsa (1987) criteria are, however, applicable because the pelican sink speeds were often less than their $0.56w_*$ threshold. Measurements of thermal updraft intensity obtained during this study were compared directly to the findings of Greenhut and Khalsa and Schumann and Moeng. Although these data are not directly comparable to that obtained by Young, the close fit of Young's data to that obtained by Schumann and Moeng allows for indirect comparison of his results. The magnitude of the profile derived from Schumann and Moeng's LES-produced estimates was less than that obtained by Greenhut and Khalsa, with the

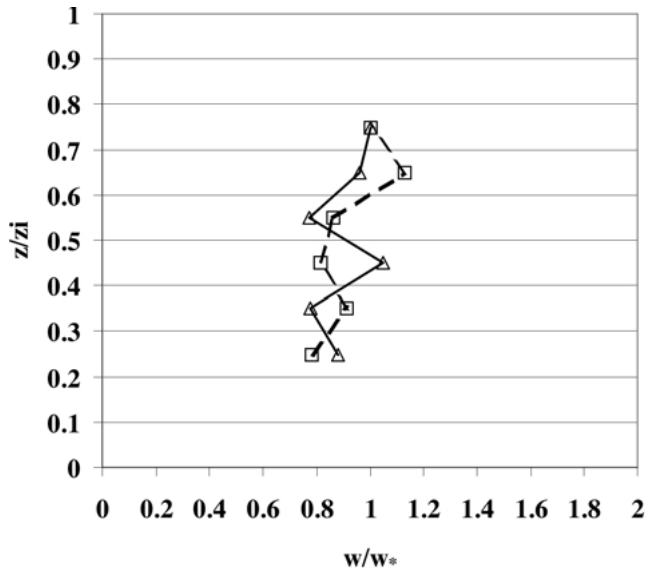

Figure 10. Normalized averaged thermal updraft intensity over the Lahontan valley (solid line) and nearby mountains (dashed line).

mean difference between these two profiles estimated at 17% ($\sigma = \pm 5\%$) between 0.2 and $0.8 z/z_i$.

Figure 11 shows the normalized profile of thermal updraft intensity obtained by applying Greenhut and Khalsa's criteria for defining thermal updrafts to the data obtained during this study. The magnitude of this profile is closer to that obtained by Schumann and Moeng (mean difference of 4%, $\sigma = \pm 11\%$) than to that obtained by Greenhut and Khalsa. In contrast, the shape of the profile is more similar to that obtained by Greenhut and Khalsa; however, slight deviations are noted near the top and bottom of the profile. Differences at the top of the profile are potentially a result of birds exiting all but the best thermals once they have enough altitude for an extended glide, a hypothesis supported by the 43% falloff in the number of measurements between the $0.4–0.5 z/z_i$ bin and the $0.7–0.8 z/z_i$ bin. Thus, data obtained near the top of the boundary layer may be representative only of the strongest thermals within the boundary layer, as opposed to the full range of resolvable thermals likely reaching that height. The similarities among these profiles over the height range 0.2 to $0.8 z/z_i$ suggests that pelican flight altitude data and model-produced estimates of boundary-layer depth and the convective velocity scale can be used to estimate thermal updraft intensity. Thus, we can indeed use these data to examine the effects of complex terrain on the vertical profile of thermal updraft intensity over the valleys and mountains within the study area.

Using LES, Gopalakrishnan et al. (2000) compare the turbulence structure of the boundary layer over a flat surface to that modelled over hillier terrain. This LES

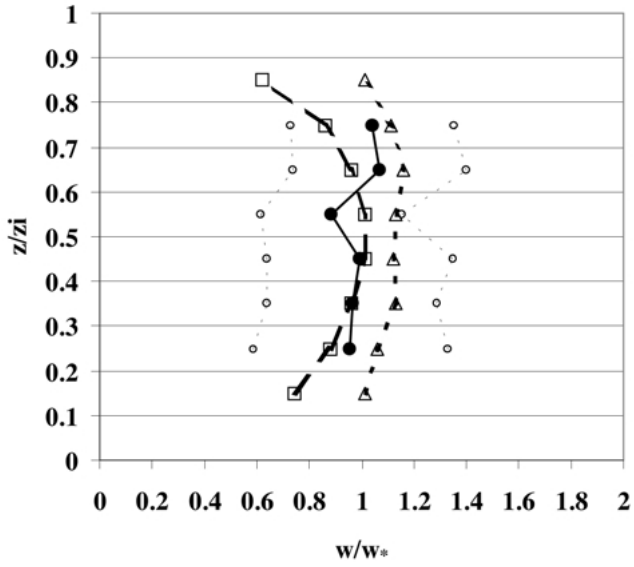

Figure 11. The normalized profile of thermal updraft intensity (solid line, circle markers) obtained by applying Greenhut and Khalsa's thresholds to data obtained during this study. The thin-dashed lines with circle markers indicate one standard deviation above and below the profile obtained during this study. Using the same criteria, the normalized profiles of thermal updraft intensity, as obtained by Schumann and Moeng (dashed line, square markers) and Greenhut and Khalsa (dotted line, triangle markers), are shown for comparison.

was configured using a sinusoidal hill with variable heights and wavelengths; the wavelengths varied from 0.9 to $7.2z_i$, with the strongest terrain effects occurring for wavelengths exceeding $1.9z_i$. Gopalakrishnan et al. show that the modelled standard deviation σ of vertical velocity over large hills (i.e., height of approximately $0.15z_i$) varied by about 11% in the middle of the boundary layer. Differences were even smaller elsewhere in the boundary layer. The results for their smaller $0.038z_i$ hills showed even less of an effect.

The mountains within the Fallon, NV area are comparable to those modelled by Gopalakrishnan et al. The heights of the small and large mountains, respectively, are approximately 0.11 and $0.23z_i$, with wavelengths ranging from 3.8 to $6.3z_i$. Figure 10 and the t-test described above demonstrate the similarity in the normalized averaged thermal updraft intensity profiles over the mountains and the Lahontan valley ($P = 0.96$). The mean difference in the magnitude of these profiles was less than 1% ($\sigma = \pm 15\%$) between 0.2 and $0.8z/z_i$. These observations support the findings of Gopalakrishnan et al., showing that the impact of terrain on thermal updraft intensity is relatively small when compared with the typical scatter associated with estimates of thermal updraft intensity obtained from aircraft measurements, LES model output, or observations of the climb rates of soaring birds within thermal updrafts. Gopalakrishnan et al. note, however, that increases in the surface buoyancy flux minimized the terrain effects of model-produced estimates of

thermal updraft intensity. The average surface potential temperature flux observed during this study was approximately 0.41 K m s^{-1}, compared with a Gopalakrishnan et al. baseline value of 0.2 K m s^{-1}. This relatively large flux is likely the reason why an even smaller difference was found between the profiles of thermal updraft intensity over the Lahontan valley and the mountains when compared with the Gopalakrishnan et al. results.

6. Conclusions

An examination of boundary-layer and avian aerodynamic theories reveals the potential value of using soaring birds to measure the vertical profile of thermal updraft intensity. These theories were applied to study the influence of complex terrain on thermal updraft intensity over a valley and nearby mountains. Thermal updraft intensity measurements derived from the climb rates of soaring pelicans were compared with those obtained in previous studies that used large research aircraft and LES to estimate thermal updraft intensity. A comparison of these data showed that pelican-derived thermal updraft intensity estimates were statistically indistinguishable from those obtained in previous studies, thus confirming that biological unmanned aerial vehicles (UAVs) can be used to study the structure of the turbulent boundary layer. An analysis of the mean profiles of thermal updraft intensity obtained over a broad valley and the nearby mountains suggested that these terrain variations had little influence on the vertical profile of thermal updraft intensity. On average, the mountains within the study area ranged from 0.11 to $0.23z_i$ in height and about 3.8 to $6.3z_i$ in width. These observations support the recent findings of Gopalakrishnan et al. (2000), who used an LES and similar terrain specifications to show that changes in the height and the width of terrain have little impact (11%) on the standard deviation of vertical velocity.

While it is possible that horizontal roll vortices were present at times during this study, observations suggest that such vortices were not a dominant feature of the convective boundary layer. Although scattered cumulus humilis were observed forming near the top of the convective boundary layer on some undisturbed days, clouds streets were not observed. Studies using motor gliders to track birds report that birds soaring cross-country can fly relatively long distances without flapping and without losing significant altitude by engaging in dolphining flight along the axis of cloud streets. The absence of cloud streets during this study does not definitively indicate that horizontal rolls were not present, however, pelicans observed soaring in approximately straight lines typically lost altitude during gliding bouts. Indeed, much less than 1% of the changes in altitude were positive between two consecutive altitude measurements when gliding flight was observed, and never were soaring pelicans observed to gain altitude beyond more than two consecutive altitude measurements. While the presence of horizontal rolls may have provided additional insight into the intensity of thermal updrafts in this regime, these rolls

may also have made it more difficult to measure the intensity of these updrafts because soaring birds tend to stay near the top of these rolls. These observations suggest that positive changes in altitude during gliding flight were likely associated with birds flying through some thermals rather than circling in each one encountered.

The results of this study demonstrate that American white pelicans can be used to measure thermal updraft intensity, however, the theories and observations of avian soaring flight suggest that other soaring species could also be used to measure this vertical velocity. The success of future studies hinges, however, on the choice of soaring species as an instrument platform. In general, the chosen species must be large enough to support an altitude-equipped radio-telemetry transmitter and engage in thermal cross-country soaring frequently enough to make instrumenting this species cost- and time-effective. Knowledge of the species' morphological characteristics is also critical to successfully apply this technique. Numerous types of eagles, hawks, vultures, and other species are potential candidates, given their tendency to soar while regularly completing long-distance foraging and migratory cross-country flights (e.g., Pennycuick, 1972). Although investigators have no way of controlling the times, altitudes, or locations that thermal updraft intensity data are available from avian soaring platforms, choosing a soaring species that is known to soar cross-country increases the chances that usable data can be obtained. The comparison of pelicans soaring cross-country versus those soaring locally during this study reinforces this conclusion. Furthermore, the avian soaring platform has several advantages over the more traditional multi-engine research aircraft used in previous studies. In contrast to the large research aircraft that employ a Eularian sampling technique to measure thermal updraft intensity, the relatively small size and maneuverability of soaring birds enables researchers to study thermal updraft intensity employing a quasi-Lagrangian sampling technique. This technique is considered quasi-Lagrangian because, while the bird is circling in a thermal updraft, it sinks relative to the upward moving air, but the bird drifts with the thermals as the thermals drift in the horizontal. An advantage of this technique over Eularian sampling is that is enables researchers to obtain thermal updraft intensity measurements from multiple heights within the same thermal. These measurements are possible because birds circling in thermal updrafts do not disturb the atmosphere significantly during their flight. These capabilities are significant because they allow researchers to study changes in thermal updraft intensity when these changes are occurring rapidly on both temporal and spatial scales.

The size and performance similarities of UAVs and soaring birds suggest that the former could be used to gather thermal updraft intensity data, provided that the UAV can be programmed to behave like a bird soaring cross-country. Such capabilities would provide investigators with another means to measure thermal updraft intensity using a quasi-Lagrangian sampling technique, while also enabling them to control the flight plan of the sampling platform. In the absence of such capabilities, the UAV still offers a means to gather such data, provided that the in-

strumentation aboard the much larger, multi-engine research aircraft can be adapted to the relatively small UAVs. Assuming that such adaptations are possible, UAVs could potentially be used to measure thermal updraft intensity through Eularian sampling as well. Finally, by equipping this vehicle with a GPS, the location of thermal updrafts could be more precisely measured relative to terrain. Such precision was not possible during this study because of limitations in the size and weight of transmitters that can be attached to soaring birds.

Acknowledgements

The authors thank Bill Henry, Robert Meese, the staff of Stillwater NWR, and the Pyramid Lake Paiute Tribe for their assistance in capturing and instrumenting the pelicans monitored during this study. The authors appreciate the efforts of Lt. Mike Nicklin and the staff of NAS Fallon meteorologists who provided meteorological data during this study. The authors also thank Kirk Bates, B. James Dayton, Paul Howey, Christopher Juckins, and Walt Wardwell for their help in tracking radio-marked pelicans. The authors especially appreciate the assistance of Colin Pennycuick who provided valuable data and insight on the aerodynamics and behavioural patterns of American white pelicans. The majority of this research was conducted at the Center for Conservation Research and Technology (CCRT) at the University of Maryland, Baltimore County (UMBC).

References

Arritt, R. W., Wilczak, J. M., and Young, G. S.: 1992, 'Observations and Numerical Modeling of an Elevated Mixed Layer', *Mon. Wea. Rev.* **120**, 2869–2880.

Bader, D. C. and McKee, T. B.: 1985, 'Effects of Shear, Stability and Valley Characteristics on the Destruction of Temperature Inversions', *J. Appl. Meteorol.* **24**, 822–832.

Banta, R. M.: 1984, 'Dry Boundary-Layer Evolution over Mountainous Terrain. Part I: Observations of the Dry Circulations', *Mon. Wea. Rev.* **112**, 340–356.

Bluth, R. T., Durkee, P. A., Seinfeld, J. H., Flagan, R. C., Russell, L. M., Crowley, P. A., and Finn, P.: 1996, 'Center for Interdisciplinary Remotely-Piloted Aircraft Studies (CIRPAS)', *Bull. Amer. Meteorol. Soc.* **77**, 2691–2699.

Crum, T. D., Stull, R. B., and Eloranta, E. W.: 1987, 'Coincident Lidar and Aircraft Observations of Entrainment into Thermals and Mixed Layers', *J. Clim. Appl. Meteorol.* **26**, 774–788.

Deardorff, J. W.: 1970, 'Convective Velocity and Temperature Scales for the Unstable Planetary Boundary Layer and for Rayleigh Convection', *J. Atmos. Sci.* **27**, 1211–1215.

Deardorff, J. W.: 1976, 'Discussion of "Thermals over the Sea and Gull Flight Behavior" by A. H. Woodcock', *Boundary-Layer Meteorol.* **10**, 241–246.

Gopalakrishnan, S. G., Roy, S. B., and Avissar, R.: 2000, 'An Evaluation of the Scale at which Topographical Features Affect the Convective Boundary Layer Using Large Eddy Simulation', *J. Atmos. Sci.* **57**, 334–351.

Greenhut, G. K. and Khalsa, S. J. S.: 1982, 'Updraft and Downdraft Events in the Atmospheric Boundary Layer over the Equatorial Pacific Ocean', *J. Atmos. Sci.* **39**, 1803–1818.

Greenhut, G. K. and Khalsa, S. J. S.: 1987, 'Convective Elements in the Marine Atmospheric Boundary Layer. Part I: Conditional Sampling Statistics', *J. Clim. Appl. Meteorol.* **26**, 813–822.
Haubenhofer, M.: 1964, 'Die Mechanik des Kurvenfluges', *Schweiz. Aerorev.* **39**, 561–565.
Holland, G. J., McGeer, T., and Youngren, H.: 1992, 'Autonomous Aerosondes for Economic Atmospheric Soundings Anywhere on the Globe', *Bull. Amer. Meteorol. Soc.* **73**, 1987–1998.
Huffaker, E. C.: 1897, 'On Soaring Flight', Smithsonian Institution, Annual Report of the Board of Regents, 183–206.
Jacks, E., Bower, B., Dagostaro, J. J., Dallaville, J. P., Erickson, M. C., and Su, J. C.: 1990, 'New NGM-Based MOS for Maximum/Minimum Temperature, Probability of Precipitation, Cloud Amount, and Surface Wind', *Wea. Forecast.* **5**, 128–138.
Khalsa, S. J. S. and Greenhut, G. K.: 1985, 'Conditional Sampling of Updrafts and Downdrafts in the Marine Atmospheric Boundary Layer', *J. Atmos. Sci.* **42**, 2550–2562.
Langford, J. S. and Emanuel, K. A.: 1993, 'An Unmanned Aircraft for Dropwindsonde Deployment and Hurricane Reconnaissance', *Bull. Amer. Meteorol. Soc.* **74**, 367–375.
Mahfouf, J.-F., Richard, E., and Mascort, P.: 1987, 'Influence of Soil and Vegetation on the Development of Mesoscale Circulations', *J. Clim. Appl. Meteorol.* **26**, 1483–1495.
Officials of the National Oceanic and Atmospheric Administration: 1974, *Climates of the States*, Weather Information Center, Inc., New York, NY, 980 pp.
Pennycuick, C. J.: 1971, 'Gliding Flight of the White-Backed Vulture *Gyps africanus*', *J. Exp. Biol.* **55**, 13–38.
Pennycuick, C. J.: 1972, 'Soaring Behaviour and Performance of some East African Birds, Observed from a Motor-Glider', *Ibis* **114**, 178–218.
Pennycuick, C. J.: 1975, 'Mechanics of Flight', in D. S. Farner and J. R. King (eds.), *Avian Biology*, New York, pp. 1–75.
Pennycuick, C. J.: 1998, 'Field Observations of Thermals and Thermal Streets, and the Theory of Cross-Country Soaring Flight', *J. Avian Biol.* **29**, 33–43.
Pennycuick, C. J., Klaassen, M., Kvist, A., and Lindström, Å.: 1996, 'Wingbeat Frequency and the Body Drag Anomaly: Wind Tunnel Observations on a Thrush Nightingale (*Luscinia luscinia*) and a Teal (*Anas crecca*)', *J. Exp. Biol.* **199**, 2757–2765.
Reichmann, H.: 1993, *Cross-Country Soaring*, Thomson Publications, Santa Monica, CA, 172 pp.
Schumann, U. and Moeng, C.-H.: 1991, 'Plume Fluxes in Clear and Cloudy Convective Boundary Layers', *J. Atmos. Sci.* **48**, 1746–1757.
Stull, R. B.: 1976, 'The Energetics of Entrainment across a Density Interface', *J. Atmos. Sci.* **33**, 1260–1267.
Stull, R. B.: 1988, *An Introduction to Boundary Layer Meteorology*, Kluwer Academic Publishers, Dordrecht, 666 pp.
Welch, A., Welch, L., and Irving, F. G.: 1977, *New Soaring Pilot*, John Murray Publishers Ltd., London, U.K., 407 pp.
Woodcock, A. H.: 1940, 'Convection and Soaring over the Open Sea', *J. Marine Res.* **3**, 248–253.
Woodcock, A. H.: 1975, 'Thermals over the Sea and Gull Flight Behavior', *Boundary-Layer Meteorol.* **9**, 63–68.
Young, G. S.: 1988, 'Turbulence Structure of the Convective Boundary Layer, Part II. Phoenix 78 Aircraft Observations of Thermals and their Environment', *J. Atmos. Sci.* **45**, 727–735.